Applied Catalysis B: Environmental 170-171 (2015) 233–240

Contents lists available at ScienceDirect

Applied Catalysis B: Environmental

journal homepage: www.elsevier.com/locate/apcatb

Nanostructured MnO_x catalysts in the liquid phase selective oxidation of benzyl alcohol with oxygen
Part II. Reaction mechanism, kinetics and deactivation pattern

Francesco Arena [a,b,*], Bianca Gumina [b], Catia Cannilla [b], Lorenzo Spadaro [b], Antonio Patti [c], Leone Spiccia [c]

[a] Dipartimento di Ingegneria Elettronica, Chimica e Ingegneria Industriale, Università degli Studi di Messina, Viale F. Stagno D'Alcontres 31, I-98166 Messina, Italy
[b] Istituto CNR-ITAE "Nicola Giordano", Salita S. Lucia 5, I-98126 S. Lucia, (Messina), Italy
[c] School of Chemistry and ARC Center of Excellence for Electromaterials Science, Monash University, Victoria 3800, Australia

ARTICLE INFO

Article history:
Received 4 December 2014
Received in revised form 23 January 2015
Accepted 30 January 2015
Available online 2 February 2015

Keywords:
MnO_x catalysts
Selective oxidation
Benzyl alcohol
Mechanism and kinetics
Stability and deactivation pattern

ABSTRACT

The mechanism and kinetics of the liquid phase selective oxidation of benzyl alcohol to benzaldehyde with oxygen on bare and Ce or Fe promoted (Mn_{at}/Me_{at}, 3) MnO_x catalysts [1] have been investigated. Irrespective of toluene as solvent, the bare and promoted catalysts drive the selective oxidation of the substrate via the Mars-van Krevelen redox mechanism due to a high reactivity of oxygen species present on the catalyst surface. The experimental 0th-order dependence on alcohol concentration signals the occurrence of a Langmuir–Hinshelwood (L–H) reaction pathway, kinetically controlled by adsorption–desorption steps (r.d.s.). Apparent 1st-order conversion trends reflect the occurrence of deactivation phenomena (i.e., parallel fouling) leading to a residual constant activity level during 50 h. DRIFT analyses of the fresh and used catalysts uncover the incipient formation of benzoic acid hindering the oxidation functionality by strong adsorption on active sites. Calcination at $T \geq 473$ K restores the functionality of the used catalysts by the removal of strongly adsorbed benzoate species.

1. Introduction

The selective oxidation of alcohols to the corresponding carbonyl compounds is a very important class of industrial synthesis reactions commonly employed to obtain a variety of chemicals for manufacturing high added-value products like drugs, vitamins, fragrances and synthetic materials [2–5]. However, the current use of special and expensive reagents for the selective oxidation of alcohols raises significant environmental and economic concerns arising from poor atom economy and high E-factor [3]. On this account, the discovery of eco-friendly heterogeneous catalytic technologies for the selective oxidation of alcohols with oxygen in absence of solvent constitutes a major green chemistry issue [3–5].

Although noble-metal catalysts are very active in the oxidation of many alcoholic substrates under mild conditions because of their noticeable O_2-activation functionality [4,6–16], high cost, deactivation phenomena and safety issues hinder their industrial applications. On account of this, Kluytmans et al. stressed the need of unconventional and innovative reactor design to avoid explosion risks and catalyst deactivation by over-oxidation and/or corrosion phenomena [17].

Despite a lower activity, bare and promoted MnO_x catalysts exhibit a highly selective activity pattern in the liquid phase aerobic oxidation of alcohols that render them a viable alternative to noble-metal catalysts [1,5,15,18–27]. Many studies on the selective aerobic oxidation of benzyl alcohol to benzaldehyde have argued that this peculiar functionality relies on enhanced oxygen mobility and high tendency of MnO_x materials to incorporate a variety of promoters and dopants improving their redox behavior [1,5,15,18–20,23,25,28–30]. Despite the advances made, decay phenomena that are detrimental to catalytic activity and the need for regeneration–rejuvenation processes have also been in this case widely documented [1,5,15,18,20,25,27].

Therefore, this work is aimed at highlighting the mechanistic aspects of the reactivity pattern of bare and promoted (Ce and Fe) MnO_x catalysts in the aerobic liquid phase selective oxidation of

* Corresponding author. Dipartimento di Ingegneria Elettronica, Chimica e Ingegneria Industriale, Università degli Studi di Messina, Italy. Tel.: +39 0906765606; fax: +39 090391518.
E-mail address: Francesco.Arena@unime.it (F. Arena).

http://dx.doi.org/10.1016/j.apcatb.2015.01.040
0926-3373/

benzyl alcohol to benzaldehyde, as previously described [1]. A simple kinetic model has allowed predictions of the catalytic behavior over a wide range of experimental conditions in agreement with DRIFT data of the fresh and used catalysts. These studies substantiate the crucial role that adsorption–desorption phenomena play in reaction kinetics and catalyst stability.

2. Experimental

2.1. Catalysts preparation

Bare (M) and Ce (M3C1) or Fe (M3F1) promoted (Mn_{at}/Me_{at}, 3) MnO_x catalysts were obtained via the previously described redox-precipitation route [1]. The main physico-chemical features of the studied catalysts are compared in Table 1.

2.2. Catalyst characterization

Diffuse Reflectance Infrared Fourier Transform (DRIFT) measurements were carried out using a Nicolet 380 Thermo Fisher spectrophotometer equipped with a smart diffuse reflectance accessory and a DTGS (deuterated triglycine sulfate) detector. Background spectra of the fresh catalysts and substrates were recorded after mixing them with KBr (≈5 wt%). Each spectrum was recorded in air in the range of 500–4000 cm^{-1} with a scan step of 8 cm^{-1}.

2.3. Catalyst testing

Catalytic tests in the aerobic liquid phase oxidation of benzyl alcohol with oxygen were carried out using into a 3-necked pyrex glass flask reactor containing a solution (V_{tot}, 50 mL) of benzyl alcohol, toluene and ethyl benzoate, used as solvent and internal standard, respectively. The alcohol concentration was varied between 0.04 and 9.70 mol/L, the last corresponding to the complete absence of solvent. The suspension was vigorously stirred, and heated at the reaction temperature under oxygen flow (60 stp mL/min). Known amounts of the powdered catalyst sample (d_p < 200 μm) were then added such that the final concentration range was 0.4–49.0 g_{cat}/L. Reusability tests were carried out on the M3F1 catalyst samples recovered after the 1st reaction cycle that were preliminarily washed with a water–ethanol solution and further subjected to thermal treatment in air for 12 h at 343 (R), 373 (C1), 473 (C2), or 673 K (C3), respectively.

3. Results and discussion

3.1. Reaction kinetics and mechanism

Although our previous study shed light onto the influence of Ce and Fe promoters on the catalytic functionality of the MnO_x catalyst [1], remarkable deactivation phenomena hinder a reliable assessment of reaction kinetics from integral conversion data obtained under std testing conditions (C_{cat}/C_{Alc}, 90 g_{cat}/mol_{Alc}) [1]. Herein, the kinetic dependence has been properly ascertained by a series of experiments conducted at different alcohol (0.04–9.7 mol/L) and catalyst (0.4–49 g/L) concentrations, the results of which are summarized in Table 2. Despite the variation in substrate concentration by more than two orders of magnitude, the initial reaction rate values ($X_{Alc}\rightarrow 0$) tightly range between 0.017 and 0.021 $mol\cdot g_{cat}^{-1}\cdot h^{-1}$, signalling negligible effects on the reaction kinetics. The measured values vary randomly around an average value of 0.019 $mol\cdot g_{cat}^{-1}\cdot h^{-1}$ and are consistent with a reaction order nearly equal to zero (Fig. 1). Moreover, considering that the maximum substrate concentration (9.7 mol/L) corresponds to pure benzyl alcohol, these data indicate the lack of "solvent-effects" which render MnO_x catalysts adequate for operations under green chemistry conditions [3].

Table 1
Physico-chemical properties of the studied catalysts (see Ref. [1]).

Catalyst	Chemical composition: atomic ratio		SA (m^2/g)[a]	PV (cm^3/g)[b]	APD (nm)[c]
	(Ce/Mn)	(Fe/Mn)			
M3C1	0.31	–	184	0.57	27
M	0	0.31	94	0.34	31
M3F1	–	0.31	136	0.38	27

[a] Surface area.
[b] Pore volume.
[c] Average pore diameter.

Table 2
Initial reaction rate values ($(rate)_{w,0}$) measured for M3F1 at different alcohol and catalyst concentrations (*T*, 343 K).

Run	C_{Alc} ($mol\cdot L^{-1}$)	C_{cat} ($g\cdot L^{-1}$)	$(rate)_{w,0}$ ($mol\cdot g_{cat}^{-1}\cdot h^{-1}$)
1	0.04	8.8	0.017
2	0.09	8.8	0.020
3	0.09	8.8	0.018
4	0.09	8.8	0.019
5	0.10	8.8	0.018
6	0.10	0.4	0.018
7	0.12	8.8	0.020
8	0.22	8.8	0.021
9	0.57	49.0	0.017
10	2.48	8.8	0.021
11	9.70	39.0	0.020

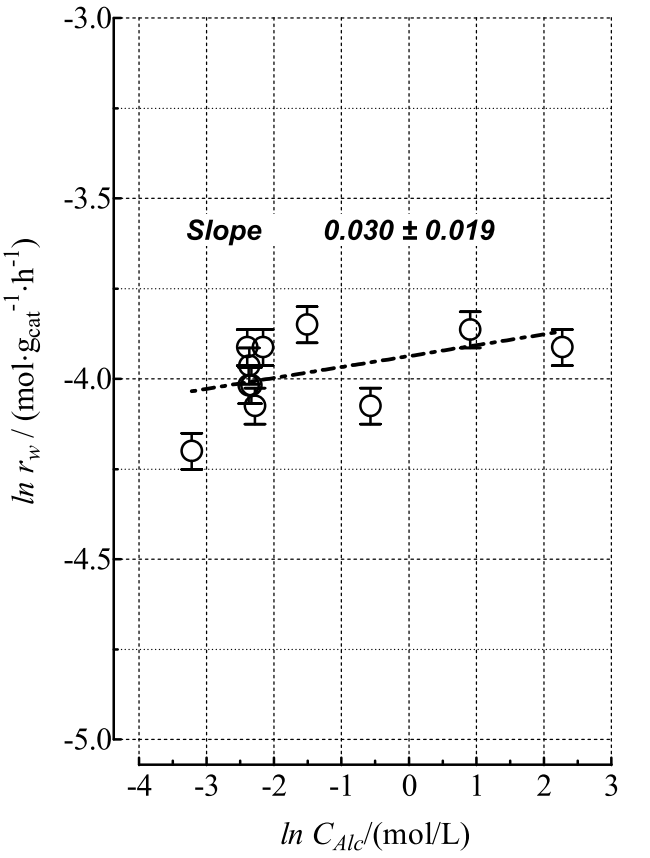

Fig. 1. Log-plot of the initial reaction rate vs. alcohol concentration (*T*, 343 K) for the M3F1 catalyst (see Table 2).

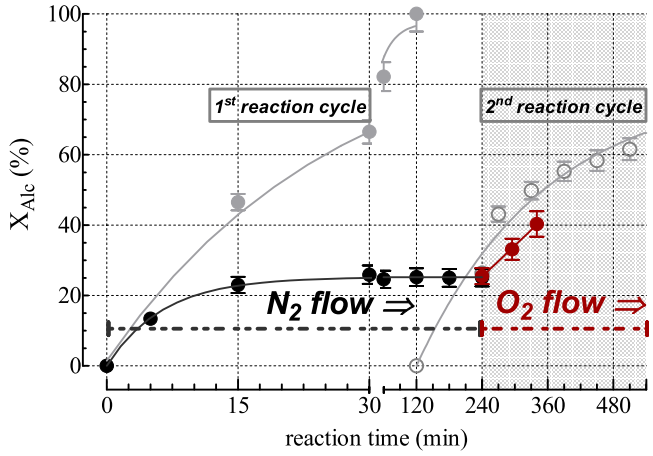

Fig 2. Benzyl alcohol conversion data for the M3C1 catalyst under N_2 and O_2 flow (T, 343 K; C_{cat}/C_{Alc}, 90 g_{cat}/mol). For reference conversion data under std reaction conditions are shown [1].

An experimental 0th-order dependence on substrate concentration is typical of a Langmuir–Hinshelwood (L–H) reaction pathway, despite previous findings providing evidence of a step-wise Mars-van Krevelen mechanism promoted by a high reactivity of surface oxygen species [18,20,25,27,30]. Thus, the reactivity of the M3C1 catalyst in absence and presence of gas-phase oxygen has been probed (Fig. 2) to shed light onto the surface reaction pathways and the origin of the above kinetic dependence [22,31].

Under a N_2 flow, the M3C1 catalyst attains a conversion degree (10–15%) in the first 5 min that well compares to that under O_2, after which it further rises to ca. 25% keeping unchanged during 4 h of reaction time (Fig. 2). This confirms the ability of oxygen species on the catalyst surface to drive the selective oxidation of the substrate, even if the amount of aldehyde produced (0.5–0.7 mmol) corresponds to an oxygen availability much lower than is required by the complete alcohol conversion (5 mmol) [1]. This finding substantiates the oxidative functionality of MnO_x materials via the redox mechanism [20,31], as confirmed by the fact that O_2 flow restores an activity comparable to that recorded in the 2nd reaction cycle (Fig. 2).

Despite having ascertained the direct involvement of catalyst oxygen in the surface reaction leading to benzaldehyde, the assessment of the rate determining step(s) (r.d.s.) is not straightforward because adsorption–desorption phenomena in the temperature range (333–353 K) of catalytic tests can well affect the reaction kinetics [32]. Thus, in addition to catalyst reduction and re-oxidation, the following reaction scheme also includes reagent-adsorption and product(s)-desorption as r.d.s.

$$C_6H_5{-}CH_2OH_{(l)} + \sigma{-}O_{(s)} \leftrightarrows C_6H_5{-}CH_2OH_{(ads)} \quad (1)$$

$$C_6H_5{-}CH_2OH_{(ads)} \rightarrow [C_6H_5{-}CHO{\cdot\cdot}H_2O{\cdot\cdot}\sigma]_{(ads)} \quad (2)$$

$$[C_6H_5{-}CHO{\cdot\cdot}H_2O{\cdot\cdot}\sigma]_{(ads)} \rightarrow C_6H_5{-}CHO_{(l)} + H_2O_{(l)} + \sigma \quad (3)$$

$$\sigma + \tfrac{1}{2}O_{2(g)} \leftrightarrows \sigma{-}O_{(s)} \quad (4)$$

Here "σ" and "$\sigma{-}O$" are the reduced and oxidized form of active sites, respectively, while "$[C_6H_5{-}CHO \cdot\cdot H_2O \cdot\cdot \sigma]_{(ads)}$" is the surface intermediate leading to the aldehyde. Assuming equilibrium conditions for the adsorption (1) and active site re-oxidation (4) steps and that steps 2 and 3 are rate determining (i.e., rate = $r_2 = r_3$) and irreversible because of the stability of (oxidation) products and slow desorption rate, respectively, the mass balance on active sites at steady-state conditions:

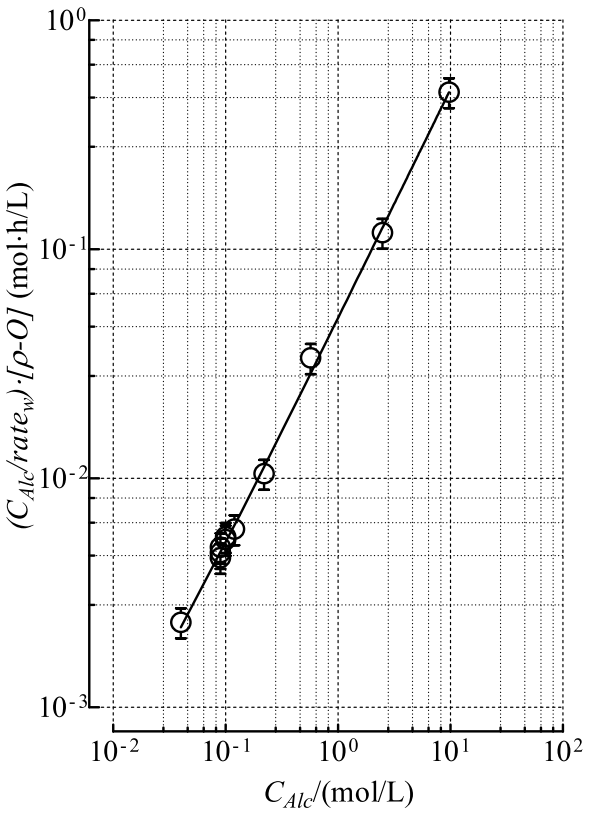

Fig. 3. Modelling of reaction rate data (Table 2) using Eq. (7).

$$[\sigma{-}O]_0 = [\sigma{-}O] + [\sigma] + [C_6H_5{-}CH_2OH]_{(ads)} + [C_6H_5{-}CHO{\cdot\cdot}H_2O{\cdot\cdot}\sigma]_{(ads)} \quad (5)$$

leads to the following rate equation

$$(\text{rate})_{w,0} = \frac{k_2 \cdot K_1 \cdot C_{Alc}}{K_1 \cdot C_{Alc}\left(1 + \frac{k_2}{k3}\right) + \left(1 + \frac{1}{K_4 \cdot C_{O2}^{0.5}}\right)} \cdot [\sigma - O]_0 (\text{mol} \cdot g_{cat}^{-1} \cdot h^{-1}), \quad (6)$$

where k_2 (h^{-1}) and k_3 (h^{-1}) are the kinetic constants of the relevant steps, K_1 (L/mol) and K_4 ($L{\cdot}mol^{-1})^{0.5}$ the equilibrium constants of alcohol adsorption and active site re-oxidation, and $[\sigma{-}O]_0$ the specific concentration of active sites ($mol{\cdot}g_{cat}^{-1}$), respectively. Despite being formally analogous to that derived from the Mars-van Krevelen mechanism [20], the 0th-order on substrate concentration would depend on a slow rate of product(s) desorption. Indeed, Eq. (7), which is the linear form of Eq. (6) (Fig. 3),

$$\frac{C_{Alc}}{(\text{rate})_{w,0}} \cdot [\rho - O]_0 = \left(\frac{1}{k_2} + \frac{1}{k_3}\right) \cdot C_{Alc} + \frac{1}{k_2 \cdot k_1} \cdot \left(1 + \frac{1}{k_4 \cdot C_{O_2}^{0.5}}\right) \quad (7)$$

provides an excellent fit ($r^2 > 0.999$) of the experimental data with slope and intercept values of $5.0{\cdot}10^{-2}$ (h) and $2.5{\cdot}10^{-4}$ ($mol{\cdot}L^{-1}{\cdot}h$), respectively. These figures confirm that the 0th-order dependence on alcohol concentration depends on a value (ca. 200) of the 1st term of the denominator of Eq. (6) much greater than the 2nd one because of larger values of the K_1 adsorption constant than the k_2/k_3 ratio and, mostly, of both k_2 and k_3 kinetic constants. Further on this account, Eq. (6) shows that the inhibiting term (denominator) consists of the cumulative contribution of the resistances of the steps 1–4 (i.e., $r_i = 1/k_i$). In particular, the 1st term of the denominator defines the small resistances of steps 1 and 4 considered at equi-

librium conditions, while the 2nd term includes the strong kinetic resistances of the steps 2 and 3, respectively. In particular, a similar rate (r.d.s.) of the latter steps implies a comparable magnitude of the relative resistances that should be in the order of ca. 0.02 h (i.e., $k_2/k_3 \approx 1$), considering the slope value ($5.0 \cdot 10^{-2}$ h) of function 7. On the other hand, an oxidation term ($K_4 \cdot C_{O2}{}^{0.5}$) considerably larger than 1 implies a K_1 value ≥100 L/mol. In this respect, it is worthy to notice that the assumption of equilibrium conditions for the step 4 does not change the core of the mechanism and the form of the relative kinetic equation (see Appendix A of SI).

Finally, an amount of surface active oxygen species corresponding to ca. 10% alcohol conversion under N_2 flow (Fig. 2) is in a good agreement with iodometric titration data of the M3F1 catalyst ($[\sigma{-}O]_0 \approx 1.0\ mmol_O \cdot g_{cat}{}^{-1}$) [27]. Used for Eq. (7) calculations (Fig. 3), this points to a remarkable TOF of ca. 20–25 h^{-1} that compares to that of Ru catalysts [4].

3.2. Deactivation pattern

Coupled to previous reusability test results, the above kinetic evidence suggests that activity decay phenomena cause remarkable deviations from 0th-order kinetics, leading to apparent 1st-order conversion trends [1,20,25]. In fact, complete alcohol conversion hides the occurrence of ongoing deactivation phenomena under std testing conditions because of the large catalyst-to-substrate ratio (C_{cat}/C_{Alc}, 90 g_{cat}/mol) [1]. Herein, the deactivation pattern of the representative M3F1 catalyst was properly probed by a series of stability tests (T, 343 K) carried out with a C_{cat}/C_{Alc} ratio of 4 g_{cat}/mol (Table 2; run 6, 10, 11). The degree of conversion under such conditions is always lower than 20% during 50 h, and does not exceed 10% during the first 6 h (Fig. 4A), in keeping with the nearly constant reaction rates for a non-deactivating system. While, the 1st derivative of the conversion curves (dX/dt) depicts analogous exponential-decay trends until a plateau is reached, which corresponds to ca. 6–7% of the initial activity level (Fig. 4B). An unchanged surface area after the 1st reaction cycle (135 m^2/g) and the activity recovery on calcination of the used catalyst at 473 K [1] suggest that the activity decay does not depend on either sintering or particle accessibility (e.g., pore plugging) [25]. Hence, the deactivation must be the consequence of a surface process somewhat inhibiting the catalytic functionality by poisoning or fouling of active sites. In fact, the exponential decay in activity (Fig. 4B) indicates a 1st-order process on reaction rate [33]

$$-\frac{d(\text{rate})_w}{dt} = k_d \cdot (\text{rate})_w \tag{8}$$

But in the light of the 0th-order dependence on alcohol concentration, the reaction rate actually reflects the concentration of active sites,

$$-\frac{d(\text{rate})_w}{dt} = k_d \cdot k' \cdot \frac{d[\sigma - O]}{dt} \tag{9}$$

where k_d and k' are the decay constant and the first term (constant) of Eq. (5), respectively. Integration between $t = 0$ and t

$$-\frac{d[\sigma - O]}{dt} = k_d \cdot [\sigma - O] \tag{10},$$

gives the final form of the equation rate

$$(\text{rate})_w = k' \cdot [\sigma - O] = k' \cdot [\sigma - O]_0 \cdot \exp(-k_d \cdot t) = (\text{rate})_{w,0} \cdot \exp(-k_d \cdot t) \tag{11},$$

which explains the observed exponential activity decay (Fig. 4B). Here, the pre-exponential term, $(\text{rate})_{w,0}$, is the initial (constant)

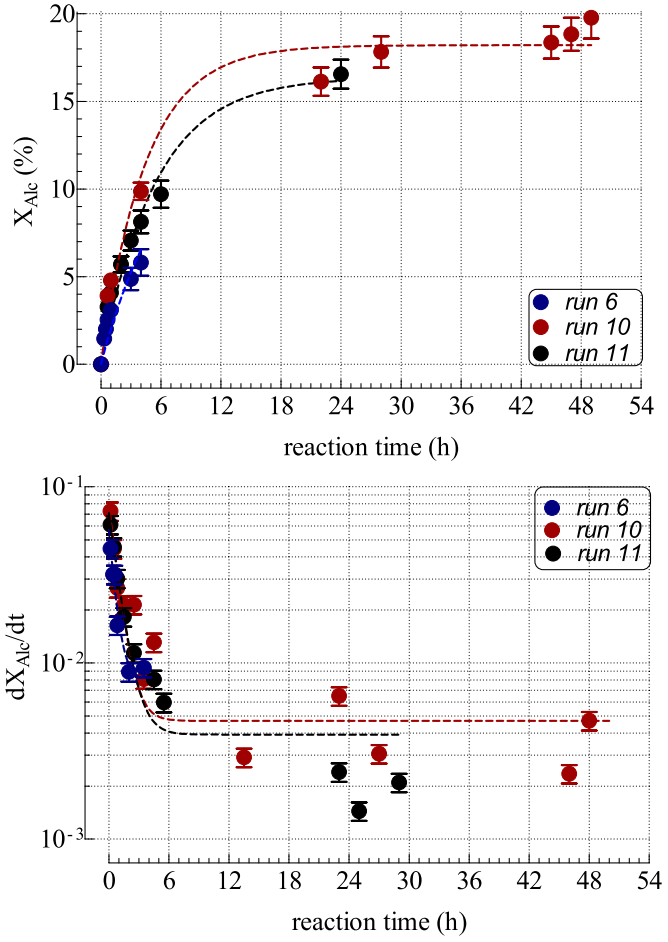

Fig. 4. (A) Activity data measured at 343 K for the M3F1 catalyst in the presence and absence of toluene as solvent (runs 6, 10, 11); (B) conversion rate vs. reaction time (runs 6, 10, 11).

reaction rate (Table 2) that, in turn, is related to the conversion rate by the following relationship:

$$\text{rate}_{conv}(h^{-1}) = (\text{rate})_w \cdot \frac{C_{cat}}{C^0_{Alc}} \left(\frac{g_{cat} \cdot L^{-1}}{\text{mol} \cdot L^{-1}} \right) \tag{12}$$

This shows that the conversion rate

$$(\text{rate})_{conv} = (\text{rate})_{w,0} \cdot \frac{C_{cat}}{C^0_{Alc}} \cdot \exp(-k_{deact} \cdot t) \tag{13}$$

matches the "dX/dt" function (Fig. 5A), while the integral between 0 and t

$$X = \left(\frac{C_{cat}}{C_{Alc}} \right) \cdot \frac{(\text{rate})w, 0}{k_{deact}} \cdot [1 - \exp(-k_{deact} \cdot t)] \tag{14}$$

matches the relative conversion trends (Fig. 5B). Curve fitting of the derivative data (Fig. 5A) was used to obtain the activity decay constant (k_d) and the pre-exponential factor values listed in Table 3. A very good agreement between the experimental and calculated pre-exponential factors substantiates the validity of the modelling. Despite the variations of C_{Alc} and C_{cat}/C_{Alc} by ca. 200 and 20 times, respectively, a fairly constant k_d value ($1.6 \pm 0.2\ h^{-1}$) is diagnostic of the same deactivation process irrespective of testing conditions.

3.3. Characterization of the used catalysts and deactivation phenomena

Although water poisoning was indicated as a potential cause of deactivation of MnO_x catalysts in the selective oxidation of benzyl

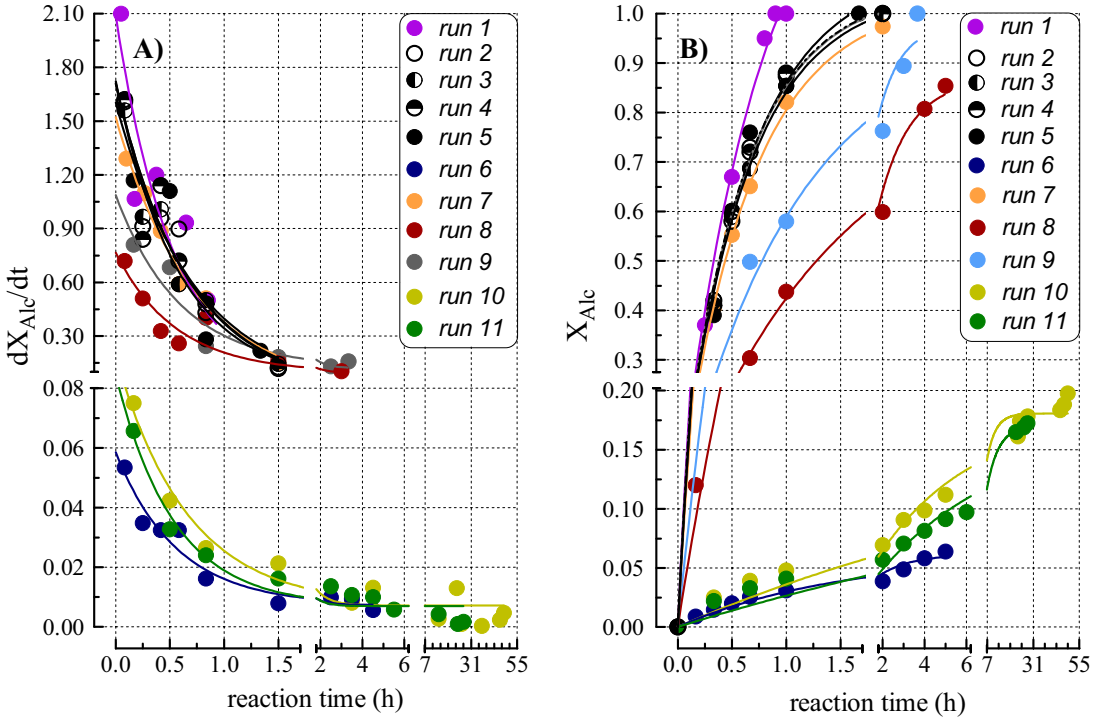

Fig. 5. Modelling of the reaction rate (A) and conversion data (B) for the M3F1 catalyst (see Table 2) obtained using Eqs. (13) and (14), respectively.

Table 3
Fitting parameters of Eq. (13) to the "dX/dt" vs. time" (Fig. 5A) data measured at different alcohol and catalyst concentrations.

Run	Experimental data		Fitting parameters	
	C_{cat}/C_{Alc} (g·mol^{-1})	$r_w \cdot (C_{cat}/C_{Alc})$ (h^{-1})[a]	$r_w \cdot (C_{cat}/C_{Alc})$ (h^{-1})	k_{deact} (h^{-1})[a]
1	205	3.9	3.5	1.6
2	97	1.8	1.9	1.5
3	95	1.8	1.7	1.7
4	94	1.8	1.8	1.5
5	91	1.7	1.6	1.4
6	4	0.1	0.1	1.8
7	77	1.5	1.5	1.4
8	40	0.8	0.8	1.8
9	87	1.7	1.5	1.7
10	4	0.1	0.1	1.5
11	4	0.1	0.1	1.8

[a] Calculated values as $C_{cat}/C_{Alc} \cdot r_w$, where $r_w = 0.019$ mol·g^{-1}·h^{-1}.

alcohol [25], water addition (mol$_{H2O}$/mol$_{Alc}$, 1) into the reaction system did not have any significant effect on the alcohol conversion rate (Fig. 6A). This is also in agreement with the fact that the used sample dried at 373 K (C1) exhibits a similar activity to that recorded in the 2nd reaction cycle (Fig. 6B) [1]. On the other hand, the used M3F1 samples calcined at 473 K (C2) and 673 K (C3) show an initial activity analogous to the fresh catalyst, indicating a major activity recovery for the C2 sample and complete recovery for sample C3, according to a conversion trend matching exactly that of the fresh sample (Fig. 6B). These findings prompted us to probe the state of the catalyst surface under reaction conditions by a systematic DRIFT study of the fresh and used samples in order to get further insights into the origin of the deactivation process. The surface reaction pattern was preliminarily assessed by analysing the fresh M3F1 sample impregnated with benzyl alcohol ($w_{Alc}/w_{cat} \approx 1$) before and after heating in air at 343 K (e.g., reaction temperature) for different times (Fig. 7). The spectrum of the bare catalyst shows very small bands at ca. 1550–1300 and 1060 cm^{-1} that can be assigned to the O—C—O [ν(COC)] and C—O

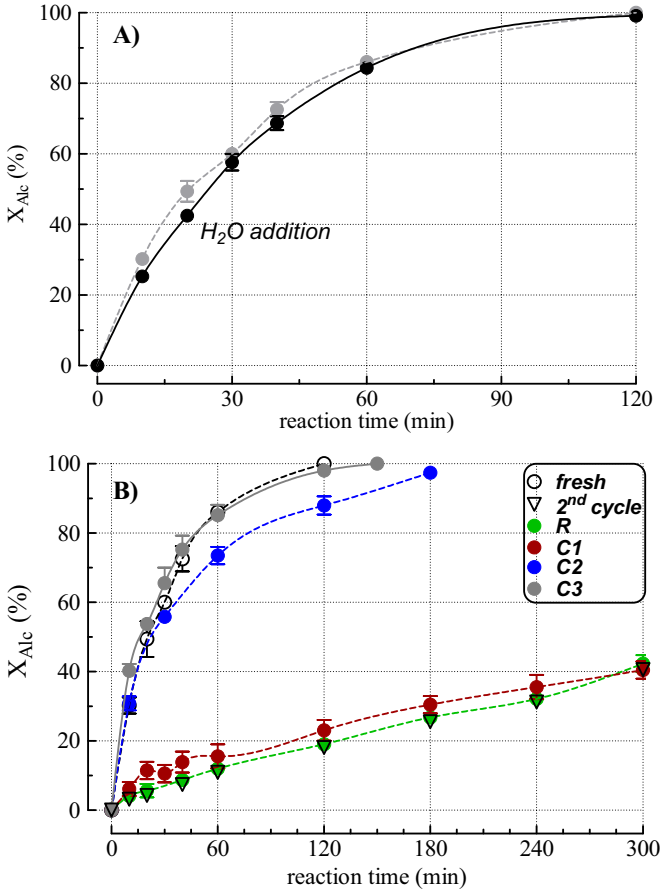

Fig. 6. (A) Benzyl alcohol conversion data measured for the M3F1 catalyst under std reaction conditions (T, 343 K; C_{cat}/C_{Alc}, 90 g$_{cat}$/mol) in presence of water (mol$_{H2O}$/mol$_{Alc}$, 1); (B) activity data for the used M3F1 catalyst samples treated in air (12 h) at 343 (R), 373 (C1), 473 (C2) or 673 K (C3).

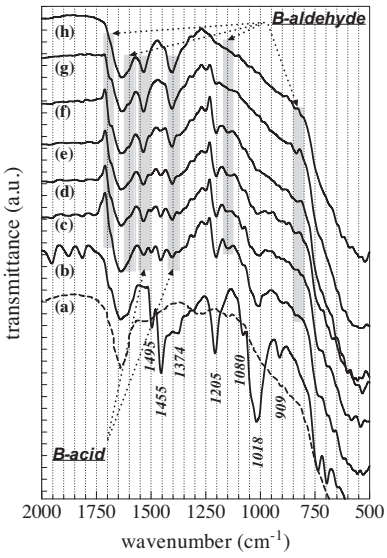

Fig. 7. DRIFT spectra for the fresh M3F1 catalyst (a), impregnated with benzyl alcohol at room temperature (b) and subsequently heated in air at 343 K for 5 (c), 10 (d), 20 (e), 30 (f), 60 (g) and 80 min (h). For reference, some characteristic signals of benzaldehyde and benzoic acid are highlighted.

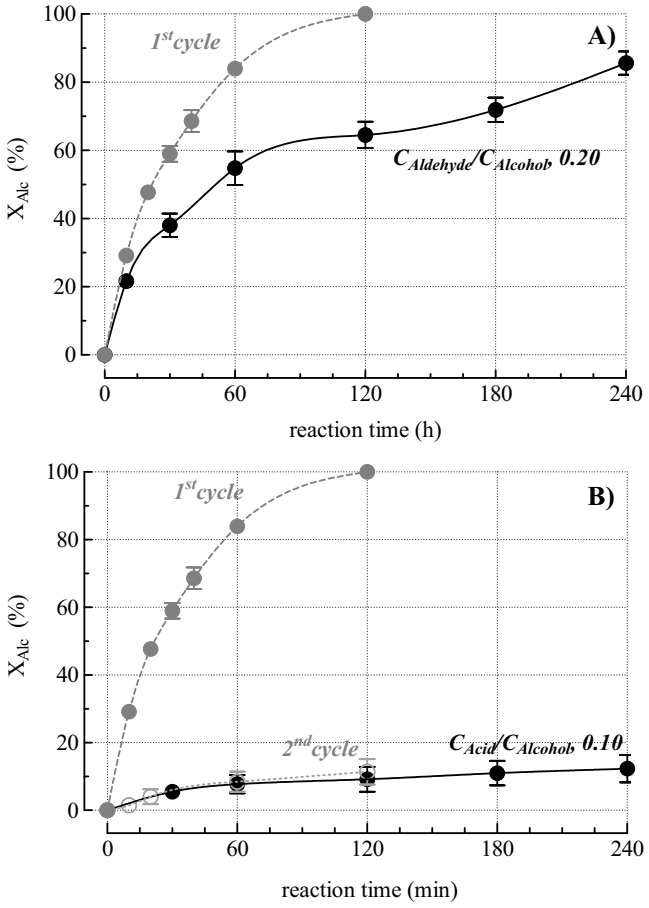

Fig. 8. Benzyl alcohol conversion data for the M3F1 catalyst measured under std reaction conditions (T, 343 K; C_{cat}/C_{Alc}, 90 g_{cat}/mol) in the presence of benzaldehyde (A) or benzoic acid (B). Activity data in the 1st and 2nd reaction cycles under std conditions are shown for reference [1].

[ν(CO)] stretching of bulk carbonates present at trace levels, while the broad band at 3000–3600 cm^{-1} (Fig. S1 of SI) is due to the OH-stretching [ν(OH)] of either bound hydroxyl groups or adsorbed water molecules and the signal at ca. 1630 cm^{-1} to the H_2O bending [$\delta(H_2O)$] [34]. The impregnated sample (Fig. 7b) shows the characteristic peaks of benzyl alcohol, consisting of two intense bands near 750 and 700 cm^{-1} due to out of plane CH bending (δ_{CH}) and four weak, though visible, absorption peaks between 2000 and 1700 cm^{-1} typical of mono-substituted aromatic compounds. In addition, the broad band at ca. 1630 cm^{-1} hides two small signals at 1610 and 1585 cm^{-1}, due to ν(C=C) and δ(C—H) vibrations of the aromatic ring, while the bands at 1495 and 1455 cm^{-1} are characteristic of skeletal vibrations. Furthermore, the signal at 1205 cm^{-1} is due to the ν(C—C) mode, whereas peaks at 1080 and 1018 cm^{-1} monitor the ν(C—O) stretching of a primary alcohol. The signal at 1374 cm^{-1} could be due to O—H in plane deformation and thus could be indicating that benzyl alcohol is adsorbed mainly in an undissociated form [35]. The characteristic peaks of benzyl alcohol (1495, 1455, 1374, 1205, 1080, 1018, 909 cm^{-1}) decrease already after 5 min at 343 K (Fig. 7c) fully disappearing after 80 min (Fig. 7h). In particular, the appearance of a broad absorption at ca. 1700 cm^{-1} along with weak signals at 1600, 1157 and 818 cm^{-1} after longer treatment times is likely to be due to the incipient benzaldehyde formation. These signals vanish in ca. 80 min (Fig. 7h). Meanwhile, two new bands at ca. 1540 and 1410 cm^{-1} due to the asymmetric ν_{asym}(COO—) and symmetric ν_{sym}(COO—) stretching of carboxylate species instantaneously appear after heating at 343 K (Fig. 7c). Their increase with treatment time indicates the progressive conversion of benzaldehyde to benzoic acid although the absence of signals characteristic of the C—O stretching (1690 cm^{-1}) and C—OH bending (1427 cm^{-1}) of the carboxylic group suggests that it is mostly in the form of adsorbed benzoate species [36]. Furthermore, the progressive decrease of the H_2O bending component at ca. 1630 cm^{-1} and the broad band between 3000–3600 cm^{-1} (Fig. S1 of SI) with treatment time likely signals a direct involvement of water in the consecutive oxidation of aldehyde, which should occur via a germinal diol intermediate undergoing a subsequent oxidative dehydrogenation to benzoic acid [1,37]. Thus, a slow oxidation of benzaldehyde to benzoic acid, remaining strongly adsorbed on active sites as benzoate species [36], is likely at the origin of catalyst deactivation (Fig. 4B). This explains the small but systematic gap in C-mass balance (ca 5%) and the small extent (ca 5%) of conversion recorded in the benzaldehyde oxidation test [1]. Catalytic tests in presence of either benzaldehyde (Fig. 8A) or benzoic acid (Fig. 8B) confirm such a hypothesis.

Although benzaldehyde (20% mol/mol) has no effect on the initial reaction rate, according to a much lower reactivity than alcohol under std testing conditions [1], the slowing down of the conversion rate after ca. 30 min probably reflects a faster formation of benzoic acid due to the higher benzaldehyde concentration (Fig. 8A). In contrast, an even lower concentration of benzoic acid (10% mol/mol) has a very strong inhibitory effect on the reactivity of the M3F1 catalyst, featuring a conversion trend analogous to that recorded in the 2nd reaction cycle under std testing conditions (Fig. 8B). These findings definitively prove the hypothesis that an incipient oxidation of benzaldehyde to benzoic acid causes the activity loss on bare and promoted MnO_x systems [1,20,25,27,28]. Indeed, the DRIFT spectra of the used M3C1 and M3F1 samples show the characteristic bands of benzoate species (1600, 1550–1540, 1410 cm^{-1}) like the M3F1 sample tested in presence of benzoic acid (Fig. 9A). Instead the spectra of the samples subjected to calcination at different temperature (Fig. 9B) show an incipient removal of the benzoate species at 473 K (C2) that is complete at 673 K (C3). This removal of benzoate species accounts for the progressive recovery in activity of the thermally treated catalyst samples (Fig. 6B).

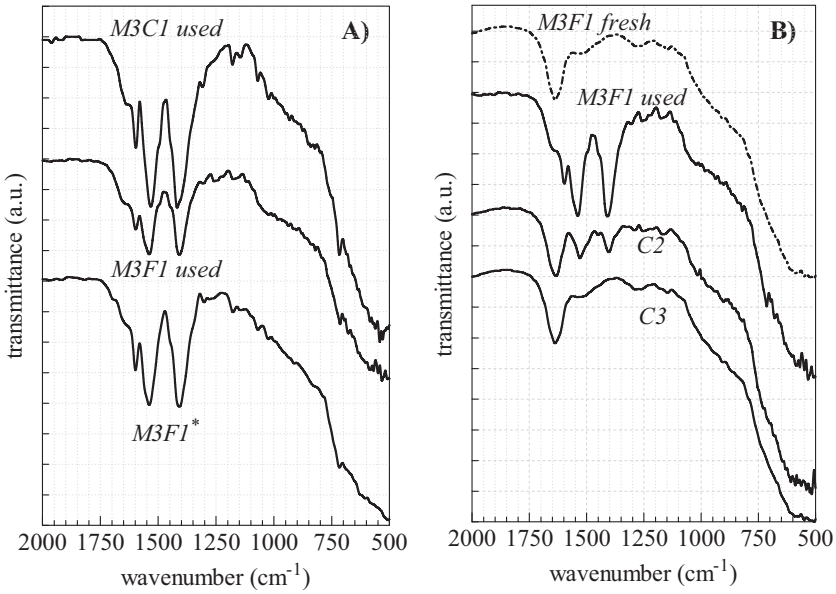

Fig. 9. DRIFT spectra of the used (A) and thermally treated (B) catalyst samples (C2, C3). The M3F1* code refers to the catalyst sample used in presence of benzoic acid (Fig. 8B).

4. Conclusions

The results of this investigation lead us to draw the following conclusions:

- Bare and promoted MnO_x systems drive the liquid-phase selective oxidation of benzyl alcohol to benzaldehyde with oxygen under mild conditions also in absence of solvent (green chemistry conditions).
- The observation of 0th-order kinetics signals the occurrence of a Langmuir–Hinshelwood reaction path under kinetic control of adsorption–desorption steps.
- Despite the independence of the reaction rate on alcohol concentration (0th-order kinetics) ongoing deactivation phenomena of bare and promoted MnO_x catalysts result in an apparent 1st-order conversion trends.
- The direct involvement of catalyst surface oxygen species in the oxidation of benzyl alcohol signals that benzaldehyde formation proceeds via the Mars-van Krevelen mechanism.
- DRIFT analyses show that the formation of minor amounts of benzoic acid is responsible for the progressive loss in activity by poisoning of active sites.
- Thermal treatment in air at $T \geq 473$ K regenerates the active sites by removing strongly adsorbed benzoate species and restores the catalytic activity.
- Future extensions of this work concern a study on “fine tuning” catalyst optimization and the influence of the reactor configuration on process performance.

Acknowledgement

LS would like to thank the Australian Research Council for financial support provided through the ARC Center of Excellence for Electromaterials Science (ACES).

Appendix A. Supplementary data

Supplementary data associated with this article can be found, in the online version, at http://dx.doi.org/10.1016/j.apcatb.2015.01.040.

References

[1] F. Arena, B. Gumina, A.F. Lombardo, C. Espro, A. Patti, L. Spadaro, L. Spiccia, Appl. Catal. B 162 (2015) 260–267.
[2] F. Brühne, E. Wright, Benzaldehyde. Ullmann's Encyclopedia of Industrial Chemistry (2000).
[3] R.A. Sheldon, I. Arends, U. Hanefeld, Green Chemistry and Catalysis, WILEY-VCH Verlag GmbH & Co. KGaA, Weinheim, Germany, 2007.
[4] T. Mallat, A. Baiker, Chem. Rev. 104 (2004) 3037–3058.
[5] C. Parmeggiani, F. Cardona, Green Chem. 14 (2012) 547–564.
[6] K. Mori, K. Yamaguchi, T. Hara, T. Mizigaki, K. Ebitani, K. Kaneda, J. Am. Chem. Soc. 124 (2002) 11572–11573.
[7] T.L. Stuchinskaya, I.V. Kozhevnikov, Catal. Comm. 4 (2003) 417–422.
[8] C. Keresszegi, D. Ferri, T. Mallat, A. Baiker, J. Catal. 234 (2005) 64–75.
[9] N. Dimitratos, A. Villa, D. Wang, F. Porta, D. Su, L. Prati, J. Catal. 244 (2006) 113–121.
[10] M. Caravati, D.M. Meier, J.-D. Grunwaldt, A. Baiker, J. Catal. 240 (2006) 126–136.
[11] M. Caravati, J. Grunwaldt, A. Baiker, Catal. Today 126 (2007) 27–36.
[12] V.R. Choudhary, R. Zha, P. Jana, Green Chem. 9 (2007) 267–272.
[13] X. Wang, H. Kawanami, S.E. Dapurkar, N.S. Venkataramanan, M. Chatterjee, T. Yokoyama, Y. Ikushima, Appl. Catal. A 349 (2008) 86–90.
[14] C.Y. Ma, B.J. Dou, J.J. Li, J. Cheng, Q. Hu, Z.P. Hao, S.Z. Qiao, Appl. Catal. B 92 (2009) 202–208.
[15] Y. Chen, H. Zheng, Z. Guo, C. Zhou, C. Wang, A. Borgna, J. Catal. 283 (2011) 34–44.
[16] P.J. Miedziak, Q. He, J.K. Edwards, S.H. Taylor, D.W. Knight, B. Tarbit, C.J. Kiely, G.J. Hutchings, Catal. Today 163 (2011) 47–54.
[17] J.H.J. Kluytmans, A.P. Markusse, B.F.M. Kuster, G.B. Marin, J.C. Schouten, Catal. Today 57 (2000) 143–1555.
[18] Y.-C. Son, V.D. Makwana, A.R. Howell, S. Suib, Angew. Chem. Int. Ed. 40 (2001) 4280–4283.
[19] H. Ji, K. Ebitani, T. Mizugaki, K. Kaneda, Catal. Comm. 3 (2002) 511–517.
[20] V.D. Makwana, Y.-C. Son, A.R. Howell, S.L. Suib, J. Catal. 210 (2002) 46–52.
[21] H. Ji, K. Ebitani, T. Mizugaki, K. Kaneda, React. Kinet. Catal. Lett. 78 (2003) 73–80.
[22] V.R. Choudhary, D.K. Dumbre, V.S. Narkhede, S.K. Jana, Catal. Lett. 86 (2003) 229–233.
[23] Y. Su, L.-C. Wang, Y.-M. Liu, Y. Cao, H.-Y. He, K.-N. Fan, Catal. Comm. 8 (2007) 2181–2185.
[24] Q. Tang, T. Liu, Y. Yang, Catal. Comm. 9 (2008) 2570–2573.
[25] F. Shurz, J.M. Bauchert, T. Merker, T. Shleid, H. Hasse, R. Gläser, Appl. Catal. A 355 (2009) 42–49.
[26] T. Sato, T. Komanoya, Catal. Comm. 10 (2009) 1095–1098.
[27] M. Ilyas, M. Saeed, Int. J. Chem. Reactor Eng. 9 (2011) 1–23.
[28] T. Qinghu, W. Chengming, H. Xiaona, Y. Yanhui, Chin. J. Catal. 30 (2009) 207–212.
[29] G. Qiu, H. Huang, S. Dharmarathna, E. Benbow, L. Stafford, S. Suib, Chem. Mater. 23 (2011) 3892–3901.
[30] X. Shen, A.M. Morey, J. Liu, Y. Ding, J. Cai, J. Durand, Q. Wang, W. Wen, W.A. Hines, J.C. Hanson, J. Bai, A.I. Frenkel, W. Reiff, M. Aindow, S.L. Suib, J. Phys. Chem. C 115 (2011) 21610–21619.

[31] A. Bielanski, J. Haber, Oxygen in Catalysis, Marcel Dekker, New York, 1990.
[32] I. Chorkendorff, J.W. Niemantsverdriet, Concepts of Modern Catalysis and Kinetics, WILEY-VCH GmbH & Co. KGaA, Weinheim, 2005.
[33] J.B. Butt, E.E. Petersen, Activation, Deactivation and Poisoning of Catalysts, Academic Press, Inc., London, 1988.
[34] F. Morales, E. de Smit, F.M.F. de Groot, T. Visser, B.M. Weckhuysen, J. Catal. 246 (2007) 91–99.
[35] M. Caravati, J.D. Grunwaldt, A. Baiker, Phys. Chem. Chem. Phys. 7 (2005) 278–285.
[36] C. Keresszegi, D. Ferri, T. Mallat, A. Baiker, J. Phys. Chem. B 109 (2005) 958–967.
[37] M. Meier, A. Urakawa, A. Baiker, J. Phys. Chem. C 113 (2009) 21849–21855.